Distribution Agreement

In presenting this thesis or dissertation as a partial fulfillment of the requirements for an advanced degree from Emory University, I hereby grant to Emory University and its agents the non-exclusive license to archive, make accessible, and display my thesis or dissertation in whole or in part in all forms of media, now or hereafter known, including display on the world wide web. I understand that I may select some access restrictions as part of the online submission of this thesis or dissertation. I retain all ownership rights to the copyright of the thesis or dissertation. I also retain the right to use in future works (such as articles or books) all or part of this thesis or dissertation.

Signature:

_____ _____

Li Yu Date

Semiconductor Nanomaterials in Photocatalytic Bipyridine Reduction and H_2 Generation

By

Li Yu
Master of Science

Chemistry

Dr. Tianquan (Tim) Lian
Advisor

Dr. Brian Dyer
Committee Member

Dr. Michael C. Heaven
Committee Member

Accepted:

Lisa A. Tedesco, Ph.D.
Dean of the James T. Laney School of Graduate Studies

Date

Semiconductor Nanomaterials in Photocatalytic Bipyridine Reduction and H_2 Generation

By

Li Yu
B.A., Peking University, 2014

Advisor: Tianquan (Tim) Lian, Doctor of Philosophy

An abstract of
A thesis submitted to the Faculty of the
James T. Laney School of Graduate Studies of Emory University
in partial fulfillment of the requirements for the degree of
Master of Science
in Chemistry
2017

Abstract

Semiconductor Nanomaterials in Photocatalytic Bipyridine Reduction and H_2 Generation

By Li Yu

Semiconductor nanoparticles have been used in the study of proton coupled electron transfer from CdS quantum dots (QDs) to N-heptyl-4,4'-bipyridinium (bPYD) and photocatalytic H_2 generation with Pt tipped CdS nanorods (NRs) under alkaline solutions. For the QDs/bPYD system, transient absorption (TA) spectroscopy was carried out to examine the pH dependence and bPYD concentration dependence of the interfacial electron and proton transfer. pH dependence experiments revealed that electron transfer happened prior to proton transfer, with the apparent electron transfer rates stayed unchanged at various pH ranging from 4 to 8. Global fitting of the concentration dependence data showed an intrinsic ET/PT rate of $7.51 \pm 0.15 \times 10^9\ s^{-1}$ at pH 8 and $4.39 \pm 0.07 \times 10^9\ s^{-1}$ at pH 5, confirming the pH independent electron transfer process. For the Pt tipped CdS NRs in photocatalytic H_2 generation, hydroxyl anions were utilized as an electron donor for fast and efficient hole removal. An external quantum efficiency of 29.3% and H_2 generation rate of 34.9 umol/h was achieved under LED light of 455 nm.

Semiconductor Nanomaterials in Photocatalytic Bipyridine Reduction and H_2 Generation

By

Li Yu
B.A., Peking University, 2014

Advisor: Tianquan (Tim) Lian, Doctor of Philosophy

A thesis submitted to the Faculty of the
James T. Laney School of Graduate Studies of Emory University
in partial fulfillment of the requirements for the degree of
Master of Science
in Chemistry
2017

Table of Contents

Figure 2.1 (A) Schematic depiction of the working principles of the QDs/bPYD system. UV-Vis absorption of CdS QDs and bPYD (B) absorption of CdS QDs and with 1 mM bPYD at pH 8. (C) absorption of CdS QDs with 5 mM bPYD, at different pH. …….5

Figure 2.2 TA spectra and trace kinetics. (A) and (C) TA spectra of CdS QDs and CdS QDs with 5 mM bPYD, at pH 8. (B) and (D) are the broadened view of (A) and (C). (E) and (F) The comparison of XB and bPYD radical signal kinetics at pH 8 and 7, separately. ……...6

Figure 2.3 Exciton bleach recovery of CdS QDs with 5 mM bPYD (A) and only QDs (B), at different pH. …….7

Figure 2.4 Panel on the left: energy diagram of the apparent equilibrium redox potential of bPYD. Panel on the right: the table of pH dependent equilibrium redox potential from molecule 1 to 4. 8

Figure 2.5 UV-Vis absorption of CdS QDs with increasing bPYD concentration at pH 8 (A) and pH 5 (B). (C) and (D) are the corresponding bleach recovery kinetics of CdS QDs. …….9

Figure 2.6 Global fitting curves of XB kinetics of CdS QDs with different bPYD concentrations, at pH 8 (A) and pH 5 (B), separately. …….....12

Table 2.1 Fitting parameters of 1S XB kinetics of free QDs[a] and m value at different bPYD concentrations, at pH 8 and 5. …….12

Figure 2.7 The average numbers of adsorbed bPYDs (m) as a function of [bPYD]. ……...13

Figure 3.1 a, b) Transmission electronic microscopy (TEM) images of CdS-Pt NRs and CdSe/CdS-Pt NRs, respectively. c) Absorption spectra of the as-synthesized nanorods and Pt tipped nanorods. Inserted is the enlarged graph at a wavelength range from 500 to 650 nm. d) Steady state PL intensities of CdS NRs and CdSe/CdS NRs. e,f) Schematic illustration of existed distinct exciton

states (X1, X2, X3) in CdS NRs and CdSe/CdS NRs. Also shown below is the simplified schematic energy levels and possible band edge transitions. ……..21

Figure 3.2 a) Schematic depicture of the photocatalytic H2 generation process b) H2 generation efficiency under different pH and second electron donors. …….23

Table 3.1 H2 generation efficiencies under different conditions. …….23

Figure 3.3 a) UV-Vis absorption of the CdS NRs after ligand exchange to aqueous solution. b) Steady state PL intensity of CdS NRs under different pH. …….25

Figure 3.4 a) PL lifetime of CdS trap emission. b) Exciton bleach (XB) feature of CdS NRs probed at 466 nm, in different pH solutions. c) Merged graph of a) & b) for better comparison. …….26

Semiconductor Nanomaterials in Photocatalytic Bipyridine Reduction and H_2 Generation

1. Introduction

Ever since the energy shortage in the 1980's, the idea of clean energy has entered the public consciousness.[1] Solar energy, among those clean, renewable energy options, stands out for its instantaneous availability and long-term sustainability. Successful utilization of this promising energy source, however, has been limited.[2] The limitation partly comes from a low energy flux density. Even though the Earth receives a huge amount of sunlight every day, the energy flow is distributed within the entire cross section of the planet, thus presenting a big challenge in efficient utilization. Another problem is the expense. Commercially available solar cell panels up to now are not really cost-effective in terms of their fabrication, installation and maintenance processes. Extensive research has been investigated into better utilization of solar energy, semiconductor based photocatalytic solar water splitting[3] and CO_2 reduction[4] has been considered as one of the most important approaches.

Semiconductor nanomaterials are promising photocatalysts mainly because of their tunable optoelectronic properties.[5-6] The absorption and photoluminescence of semiconductor quantum dots (QDs) can be readily tuned by altering the particle size, for example. By

optimizing the size and morphology, semiconductor nanomaterials can absorb at the UV-Vis region where consists half of the sunlight energy and provide the right onset potential for efficient H_2 generation or CO_2 reduction.

This thesis explores some of the fundamental processes in the photocatalytic solar energy conversion. In chapter 2, CdS QDs are used in the photo reduction of N-heptyl-4,4'-bipyridinium, which mimics one of key steps in the photocatalytic CO_2 reduction in some pyridine or its derivatives related reaction systems. Chapter 3 deals with photocatalytic H_2 generation using Pt tipped CdS nanorods under alkaline solutions. CdS nanorods here serve as the light absorbing material and Pt functions as a cocatalyst for proton reduction.

2. Proton Coupled Electron Transfer from Quantum Dots

2.1 Introduction

CO_2 reduction and fixation has been an intense research field for a few decades because of the public insights into global climate change and renewable energy storage.[7] Both electrochemical and photoelectrochemical approaches[8] have been investigated to help advance the understanding of CO_2 reduction photocatalysts and energy conversion efficiency. Bocarsely and coworkers have achieved selective photoreduction of CO_2 to methanol with a catalyzed p-GaP or Pt electrodes.[9-10] Flake and coworkers reported recently about the electrochemical reduction of CO_2 at functionalized Au electrodes.[11] Pyridine derivatives were proposed to have played an important role in the shuttling of electrons and protons. In fact pyridinium and its derivatives have found more place in the more homogeneous catalytic CO_2 reduction, though the mechanism involving pyridinium cations and their corresponding pyridinyl radicals were still under debate.[12-13]

Apart from the theoretical controversy, direct experimental confirmation of the pyridinyl radicals and their reaction activities in the electrode molecule interface or its homogeneous solution counterpart is also inadequate. In sight of this, Chen has studied the proton coupled electron transfer (PCET) from CdSe quantum dots (QDs) to 4,4'-bipyridine in aqueous solution.[14] The choice of CdSe semiconductor QDs can well mimic the electrode solution interface with tunable conduction band levels, due to quantum confinement effect.[6]

Through transient absorption (TA) and static absorption experiments, the reduction of bipyridine was found to be a PCET pathway happened at the interface of CdSe QDs and adsorbed bPYD molecules. Given the discovery that proton transfer coupled as a successive reaction after electron transfer, it is more intriguing to observe a concerted electron proton transfer in a QDs-molecule interface. Since bPYD exits in multiple protonation states (bPYD, $bPYDH^{+}$, $bPYDH_2^{2+}$) in the working pH range (4-7), it adds to the complexity of analyzing the electron transfer situations from QDs. We have thus chosen N-heptyl-4,4'-bipyridinium (we also denote it as bPYD hereafter) instead of bipyridine to study its reduction reaction with CdS QDs. Since one side of the bipyridine molecule is ended with a heptyl group, only the other side can be possibly protonated. As depicted in Figure 2.1(A), photoexcited CdS QDs will deliver an electron to bPYD, while proton transfer should happen on the same side of molecule. TA experiments in the pH dependence and bPYD concentration dependence showed that bPYD reduction was an interfacial PCET reaction pathway.

2.2 Results and Discussion

UV-Vis absorption: The UV-Vis absorption spectra of CdS QDs with bPYD is shown in Figure 2.1(B). CdS has a prominent absorption peak at around 460 nm, which can be attributed to its 1S exciton band. The average size of the CdS QDs can be calculated to be 5.7 nm, based on previous work by Peng and coworkers.[15] The 1 mM bPYD absorbs in the UV region of 280 nm and the absorption of CdS and bPYD at pH 8 can be considered as the linear combination of both CdS and bPYD. Whereas the absorption will experience an upshift due to the aggregation of QDs at lower pH or higher bPYD concentration, as is

shown in Figure 1(C). 5 mM of bPYD will lead to the aggregation of CdS QDs and thus long tail scattering, regardless of the solution pH.

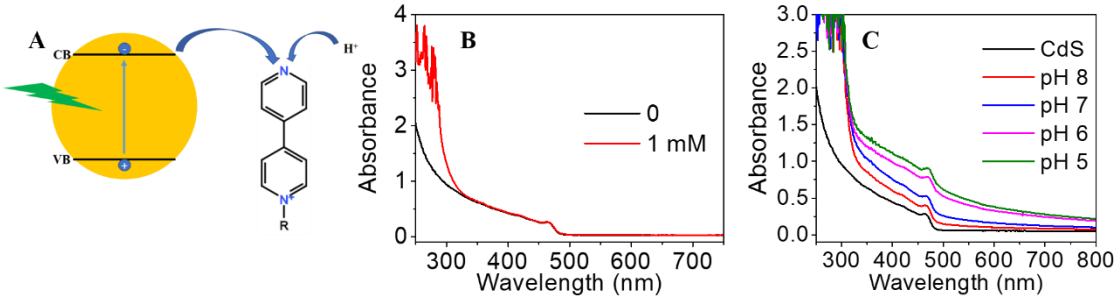

Figure 2.1 (A) Schematic depiction of the working principles of the QDs/bPYD system. UV-Vis absorption of CdS QDs and bPYD (B) absorption of CdS QDs and with 1 mM bPYD at pH 8. (C) absorption of CdS QDs with 5 mM bPYD, at different pH.

Transient absorption (TA) study of CdS QDs and bPYD – pH dependence: Charge transfer kinetics from CdS QDs to bPYD were studied by transient absorption measurements. Figure 2.2 shows the typical TA spectra of free CdS QDs in water and QDs/5mM bPYD under pH 8. The bleach at around 460 nm corresponds to the state filling of 1S exciton level, which provides a convenient way to observe the behavior of excited electrons in CdS conduction band. The lifetime of these excited electrons can be as long as 100 ns before charge recombination or interfacial charge transfers. The enlarged view of TA spectra from 500 to 700 nm shows the appearance of bPYD radical, which has a broad absorption in the visible range centered at 600nm.[16] The rise of bPYD radical signal and the decay of CdS excitons are also compared that they overlap at the beginning 1 ns, suggesting that photo generated electrons are transferred from CdS QDs to bPYD.

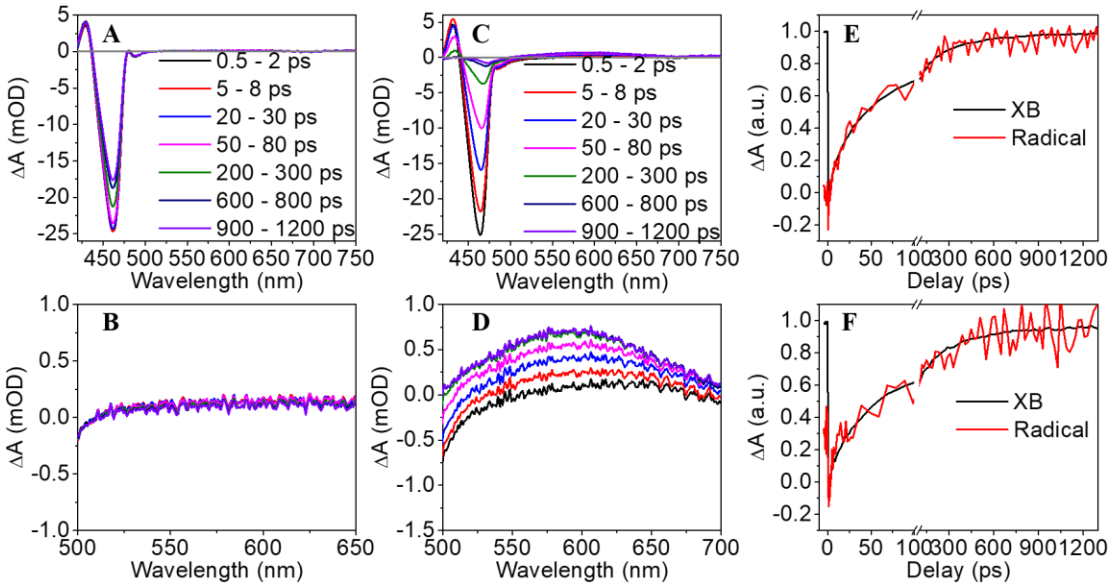

Figure 2.2 TA spectra and trace kinetics. (A) and (C) TA spectra of CdS QDs and CdS QDs with 5 mM bPYD, at pH 8. (B) and (D) are the broadened view of (A) and (C). (E) and (F) The comparison of XB and bPYD radical signal kinetics at pH 8 and 7, separately.

The charge transfer rate in different pH was also studied, ranging from pH 4 to 8, in Figure 2.3. The two graphs displayed are the XB recovery kinetics of CdS QDs with 5 mM bPYD and without bPYD, separately. The set of control experiments of free CdS QDs under the specified pH range was carried out that showed solution pH won't affect the exciton lifetime of CdS QDs. All the QDs have an exciton half lifetime of 7.5 ± 0.2 ns, as was read when kinetic trace decay to half of the initial amplitude. There was also no significant difference in the electron transfer rate from CdS QDs to bPYD. It can be explained by the energy diagram of the apparent equilibrium redox potentials between different bPYD species in Figure 4. One thing need to note is that the bPYD molecule shown in the figure is N-methyl-4,4'-bipyridinium, the electrochemical properties have been reported previously.[16-17] The actual molecule studied in this work is N-heptyl-4,4'-bipyridinium.

Different reduction and protonation states of bPYD were marked as a list of numbers, where 1 represents the original bPYD molecule, 4 is the protonated bPYD radical $bPYDH^{+\cdot}$. E(1/4) in the table means the apparent equilibrium conversion potential from 1 to 4, at different pH. The standard redox potential of $E^{\circ}(1/4)$ is -0.21 V, but solution pH will affect the apparent halfway potential in the manner of $E(1/4) = -0.21 - 0.059 \times pH\ (V)$. Since the pKa of molecule (4/3) is 10.4 and it's bigger than the pH studied in this work, we could assume that the final reduction product of bPYD is the protonated radical $bPYDH^{+\cdot}$.

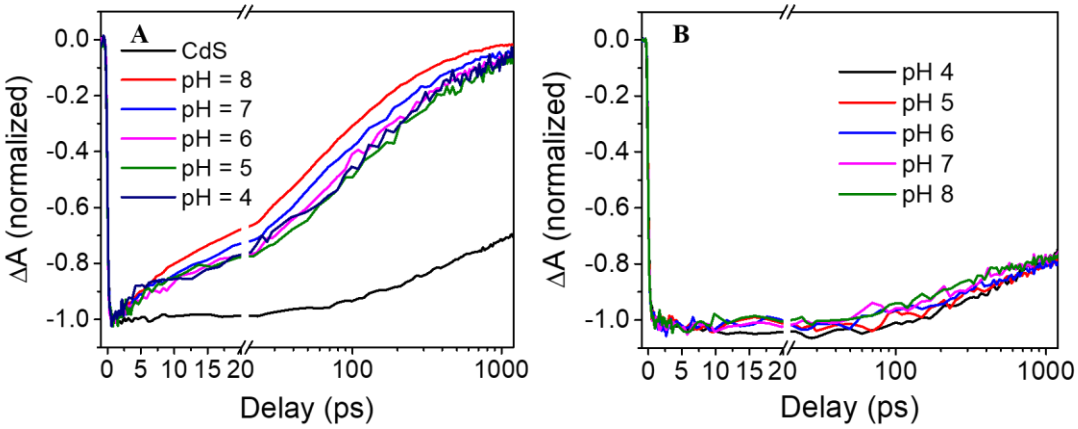

Figure 2.3 Exciton bleach recovery of CdS QDs with 5 mM bPYD (A) and only QDs (B), at different pH.

The reaction pathway from bPYD(1) to $bPYDH^{+\cdot}$(4) has three possibilities, from the energy diagram. They are 1-3-4, 1-4 and 1-2-4, namely ET-PT, EPT, PT-ET. They are all energetically allowed, but the fact that pKa(2/1) is 3.0 will make bPYD unlikely be protonated at pH 7 or 8, the reaction pathway 1-2-4 can be ruled out. We already know that the apparent halfway reaction potential E(1/4) depends on pH but electron transfer rate or the reduction rate stays unchanged, we can thus conclude that the conversion of 1 to 4

proceeds in the route 1-3-4. This way, the electron transfer happens prior to proton transfer and won't be affected by solution pH. The electron transfer observed in the TA will be from CdS QDs to bPYD to yield $bPYD^{-\cdot}$.

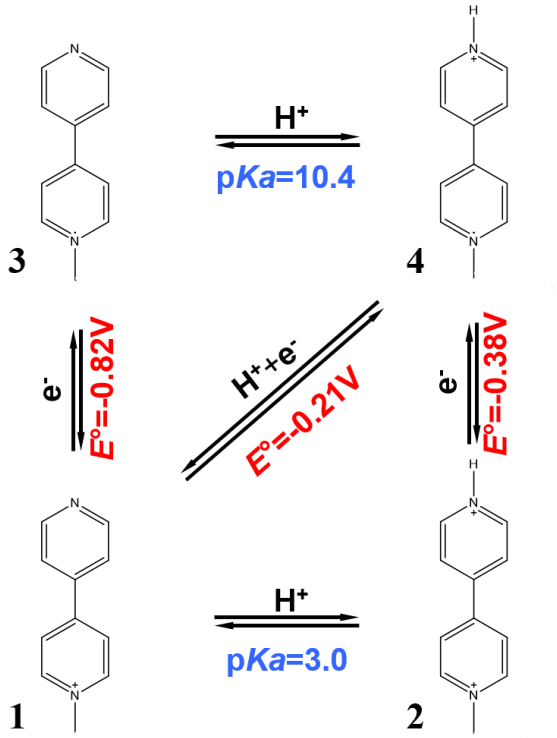

pH	E(1/4)/V
4	-0.45
5	-0.51
6	-0.56
7	-0.62
8	-0.68
9	-0.74

Figure 2.4 Panel on the left: energy diagram of the apparent equilibrium redox potential of bPYD. Panel on the right: the table of pH dependent equilibrium reaction potential from molecule 1 to 4.

bPYD concentration dependence of charge transfer rates: The bPYD molecules in solution should have two states: either adsorbed on the surface of QDs or freely dispersed in bulk solution. To examine whether the electron transfer from QDs happens on the adsorbed QDs or dispersed bPYD, we carried out bPYD concentration dependence experiments. As is shown in Figure 5, we explored a bPYD concentration range from 0.05 mM to 10 mM, both in pH 5 and 8. The apparent electron transfer rate increased upon increased bPYD concentration and reached its maximum at higher concentrations. This

trend can be explained by the increased adsorbed bPYD molecules upon increasing concentration and the maximum electron transfer rate was due to the saturated adsorption of molecules on QDs surface. On the other hand, increasing bPYD concentration can also increase the freely dispersed molecule concentration and thus increase the apparent electron transfer rate. This relationship, however, should be linear and the charge transfer rate should not reach a maximum until bPYD saturated in water, if QDs to bulk bPYD is the electron transfer pathway. Based on the above reasoning, we can safely conclude that it is the interfacial electron transfer from CdS QDs to adsorbed bPYD molecules.

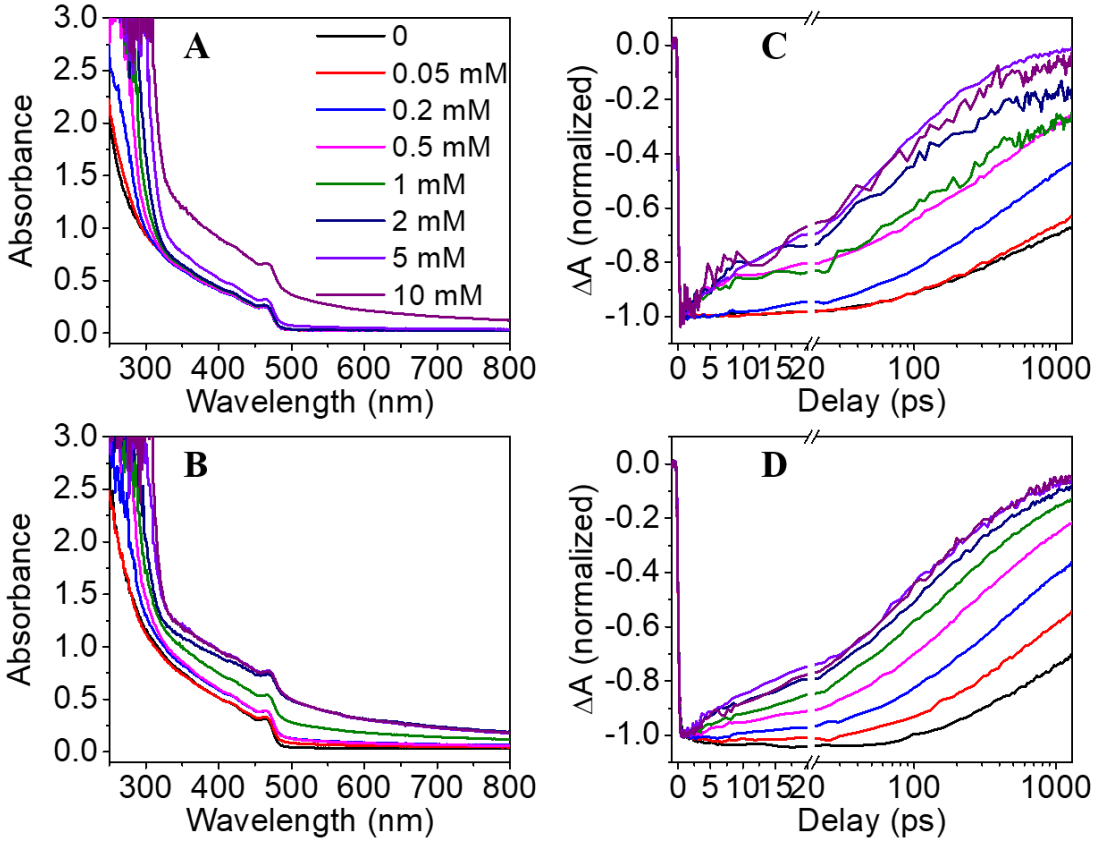

Figure 2.5 UV-Vis absorption of CdS QDs with increasing bPYD concentration at pH 8 (A) and pH 5 (B). (C) and (D) are the corresponding bleach recovery kinetics of CdS QDs.

To verify that proton transfer is coupled with electron transfer, both pH 5 and 8 were studied in the set of bPYD concentration experiments. We could see that both pH conditions yielded similar electron transfer rate increasing trend, but differed at the beginning bPYD concentration. The exciton bleach recovery kinetics were close to each other at free QDs and QDs with 0.05 mM bPYD at pH 8, meaning little electron transfer happened. Whereas in the case of pH 5, 0.05 mM bPYD led to an obvious faster bleach recovery of the CdS QDs excitons. This difference suggests the role of proton transfer in the electron transfer kinetics, though the reason behind it is still unclear.

Intrinsic electron transfer rate (k_{int}) from CdS QDs to bPYD: We have observed similar electron transfer rates at different solution pHs, when bPYD concentration was 5 mM and increasing apparent ET/PT rates at increasing bPYD concentrations. The determination of concentrations here likely implies that there were increasing average number of adsorbing bPYD molecules on CdS QDs when bulk bPYD amount increased in solution. The apparent electron transfer rate can be expressed as the sum of each single electron transfer from QD to bPYD:

$$k_{app} = -nk_{int} \quad (1)$$

The k_{int} and k_{app} here represents the intrinsic and apparent electron transfer rate from QDs to bPYD, with n be the average number of adsorbed bPYD molecules per QD. We need to obtain the intrinsic electron transfer rate from the apparent rate, in order to better compare the different electron transfer rates in the concentration and pH dependence experiments.

Previous studies in single QD[18] and multi QDs ensembles[19-20] have shown that adsorption of molecules on QDs follows the Poisson distribution. The probability of having n adsorbed molecules per QD obey the following relationship:

$$P(n,m) = \frac{m^n e^{-m}}{n!} \tag{2}$$

Where m is the average number of adsorbed molecules in a multiple QDs/molecules ensemble. The ensemble averaged 1S exciton bleach (XB) recovery kinetics can be expressed like this:

$$N(t,m) = N(0)[\sum_n e^{-nk_{int}t} P(n,m)] S_{free}(t)$$

$$= N(0)\left[e^{m(e^{-k_{int}t}-1)}\right] S_{free}(t) \tag{3}$$

Here $S_{free}(t)$ is the XB kinetics of free CdS QDs without any bPYD molecules, it can be independently acquired by fitting the decay trace of free CdS QDs. $N(t,m)$ and $N(0)$ are the exciton population at time t and 0. If we move the term $N(0)$ from right to the left side, we will find $N(t,m)/N(0)$ depicts the XB kinetics of CdS QDs with bPYDs. We can then use the above equation to globally fit the concentration dependent XB kinetics at pH 8 and pH 5. The fitting curves are shown in Figure 6 (fitting curves don't match the original data very well in pH = 8, may be due to the lack of good experimental control). From the global fit we can get the two fitting parameters k_{int} and m, they are displayed in Table 1. The three exponential decay fitting results of free QDs at pH 8 and 5 are also included. The intrinsic ET/PT rate (k_{int}) at pH 8 is $7.51 \pm 0.15 \times 10^9\ s^{-1}$ and pH 5 is $4.39 \pm 0.07 \times 10^9\ s^{-1}$, which are in the same order, confirming the fact that the intrinsic electron transfer rate from CdS QDs to bPYDs is independent of solution pH and bPYD

concentration. The different apparent electron transfer rates in the concentration dependence experiments can be accounted as the different adsorbed amount of bPYD molecules, whereas the same bPYD concentration will lead to the same apparent ET rate, regardless of solution pH.

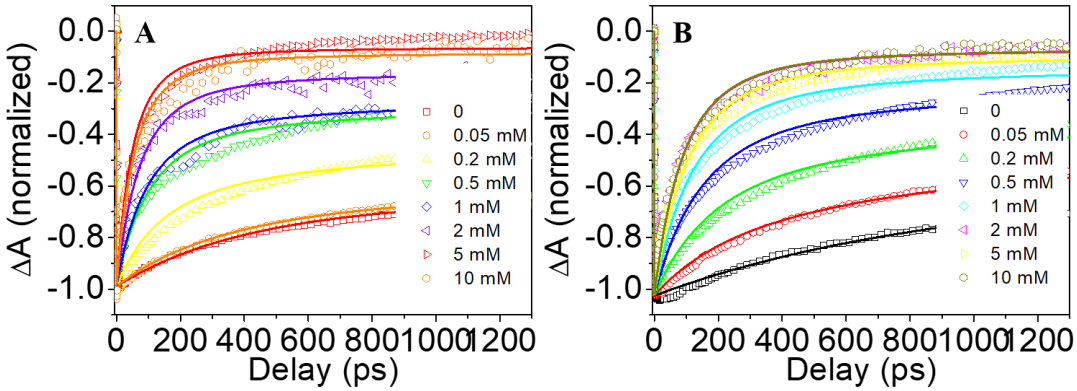

Figure 2.6 Global fitting curves of XB kinetics of CdS QDs with different bPYD concentrations, at pH 8 (A) and pH 5 (B), separately.

Table 2. Fitting parameters of 1S XB kinetics of free QDs[a] and m value at different bPYD concentrations, at pH 8 and 5.

	A_1	τ_1/ps	A_2	τ_2/ps	A_3	τ_3/ps	
pH = 8	-0.28	375 ± 20	-0.30	8776 ± 178	-0.41	43101 ± 916	
pH = 5	-0.41	905 ± 26	-0.015	1244 ± 59	-0.60	78400 ± 1534	
m	**0.05 mM**	**0.2 mM**	**0.5 mM**	**1 mM**	**2 mM**	**5 mM**	**10 mM**
pH = 8	0.028 ± 0.005	0.308 ± 0.007	0.744 ± 0.011	0.826 ± 0.012	1.38 ± 0.02	2.31 ± 0.04	2.02 ± 0.03
pH = 5	0.213 ± 0.006	0.541 ± 0.008	0.977 ± 0.012	1.43 ± 0.02	2.18 ± 0.03	1.84 ± 0.03	2.20 ± 0.03

[a]The function used to fit the XB kinetics is $\Delta A(t) = \sum_{i=1}^{3} A_i e^{-\frac{t}{\tau_i}}$

The m value obtained from the global fitting shows the average number of adsorbed bPYD molecules under a given concentration, which should have a Langmuir adsorption isotherm[20] relationship with bulk concentration [bPYD]:

$$\theta = \frac{m}{A_0} = \frac{k_f[bPYD]}{1+k_f[bPYD]} \quad (4)$$

Where A_0 is maximum binding sites per QD and θ is the mean fractional surface coverage of bPYD species on QDs. k_f is the binding constant of bPYD on QD surface. The data points of m and [bPYD] are ploted in Figure 7, with fitting curves based on Langmuir relationship.

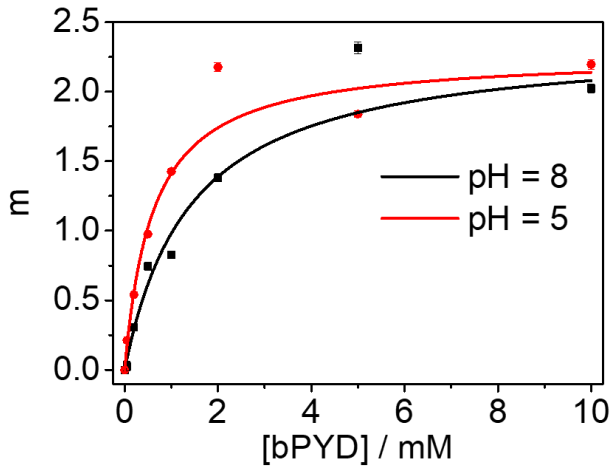

Figure 2.7 The average numbers of adsorbed bPYDs (m) as a function of [bPYD].

The fitting results reveal that the maximum binding sites on CdS QDs is about 2. The binding constant of bPYD with CdS QDs is about $700 \pm 160\ M^{-1}$, which is comparable and consistent with previous results of bipyridine ($112\ M^{-1}$) and methyl viologen ($1192\ M^{-1}$) with CdSe QDs.[14]

2.3 Conclusion

We have observed proton coupled electron transfer reactions in the CdS/bPYD bimolecular systems, through transient absorption studies. Proton transfer occurred successively after electron transfer from photoexcited CdS QDs to surface adsorbed bPYD molecules. Given the same bPYD concentration, electron transfer rates stayed unchanged at various solution pH, suggesting the direct reduction of bPYD to $bPYD^{-\cdot}$, without proton transfer involved in this step. The apparent electron transfer rates increased upon increasing bPYD concentrations until reached their maximum at 5 mM. Through the global fitting of this concentration dependence experiment data, intrinsic electron transfer rate (k_{int}) was found to be $7.51 \pm 0.15 \times 10^9\ s^{-1}$ at pH 8 and $4.39 \pm 0.07 \times 10^9\ s^{-1}$ at pH 5, confirming the pH independent electron transfer process. Further analysis of the average adsorbing molecules on CdS QDs at different bPYD concentrations revealed that they obey the Langmuir isotherm surface coverage relationship, with the maximum binding sites on CdS QDs to be 2 and the binding constant with bPYD to be $700 \pm 160\ M^{-1}$. The mechanism of proton coupled electron transfer from CdS QDs to bPYD molecules in this work will provide insights into the exploration of the role of pyridine and its derivatives in the photoelectrochemical reduction of CO_2 and also interfacial concerted proton electron transfer reactions.

2.4 Sample Preparation and Transient Absorption Spectroscopy Setup

Synthesis of CdS Quantum dots: CdS nanoparticles were synthesized based on previously reported literature.[21] Typically, 512 mg of cadmium oxide (CdO), 5 ml of oleic acid (OA) and 15 ml of octadecene (ODE) were mixed in a 50 ml three-neck flask. The

mixture was degassed for 1 hour under vacuum and then heated up to 270 ℃ to let CdO completely dissolve. The temperature was stabilized at 250 ℃ for injection of the sulfur precursor containing 128 mg of S and 2 ml of trioctylphosphine (TOP). Reaction was stopped by water bath, after 5 mins (time can be tuned to achieve desired particle size). The resulting CdS QDs were washed out by adding toluene and acetone for centrifuge. Finally the CdS QDs were stored in hexane for later use.

Ligand exchange for water soluble CdS quantum dots: The hydrophobic ligands of CdS QDs need to be replaced by some hydrophilic molecules, which is 3-mercaptopropionic acid (MPA) here. About one-tenth of the as-synthesized nanoparticles were added to 10 ml of methanol, with 25 µl of MPA. The pH of MPA/methanol solution is tuned to be over 10, with tetramethylammonium hydroxide. The mixture was let stir for 2 hours and then 10 ml of water was added and stirred for another 10 mins. The final solution was let stand over night to allow for phase separation. The water phase was taken out and centrifuged with 10 ml of acetone. CdS QDs were dispersed in water and stored in refrigerator.

Sample solution preparation: CdS QDs water solution is diluted to the desired CdS QDs concentration and then mixed with bPYD water solution. The solution pH was adjusted by HCl and KOH. Solution degassing was sometimes needed.

Femtosecond transient absorption: The setup is based on a Helios spectrometer with a regenerative amplified Ti:sapphire laser system (Coherent Legend, 800 nm, 150 fs, 3 mJ/pulse, and 1 kHz repetition rate). A small part (7%) of the 800 nm laser beam is frequently doubled by a BBO crystal to generate a 400 nm laser beam. A series of neutral-density filters are used to adjust the pump laser beam. The pump beam is finally focused on the sample with a waist width of 300 nm. The continuous white light from 420 to 800

nm, which is used as the probe beam and also reference beam, is generated by focusing ~10μJ of the 800 nm pulse into a sapphire window. The probe beam is focused with an Al parabolic reflector onto the sample with a beam waist of 150 nm. Both the reference and probe beams are sent into a fiber optics-coupled multichannel spectrometer with complementary metal-oxide-semiconductor (CMOS) sensors and detected at a frequence of 1 kHz. The ratio between the intensities of reference and probe beams are adjusted to compensate the pulse-to-pulse fluctuations. The pump beam is chopped by a synchronized chopper to 500 Hz. The delay time between the pump and probe pulses is controlled by a motorized delay stage. 2 mm cuvettes are used in all solution sample measurements. The instrument response function (IRF) of this system is about 150 fs, as was measured previously.[22]

Nanosecond transient absorption: Visible ns TA is performed with the EOS spectrometer (Ultrafast Systems LLC). The 400 nm pump laser pulses are generated in the same way as in the fs TA setup. The white probe light (380-1700 nm, 0.5 ns pulse width, 20 kHz repetition rate) is generated by focusing a Nd:YAG laser into a photonic crystal fiber. The delay time between pump and probe beams is controlled by a digital delay generator (CNT-90, Pendulum Instruments). The reference and probe pulses are detected with the same multi-channel spectrometers as in the fs TA experiments. The femtosecond TA data and the nanosecond TA data can be jointed at a delay time windows from 0.5 to 1 ns.

3. Photocatalytic H_2 generation Using Pt-tipped CdS Nanorods

3.1 Introduction

Hydrogen has been regarded as a clean and sustainable energy source[23] to address the issue of climate change[24] and fossil fuel shortage[25]. In this respect, some approaches have been developed to generate hydrogen, of which semiconductor based photocatalytic hydrogen evolution was pioneered by Fujishima and co-workers in 1972.[26] They used n-type TiO_2, the most intensively investigated semiconductor material since then,[27] as the working electrode to absorb light and pass on photon-excited electrons to Pt electrode for hydrogen generation. Some other metal oxides, like La doped $NaTaO_3$,[28] has achieved a high water splitting quantum yield of 56%. These metal oxides, however, are not active in the visible light region which compose almost half of the sun light. CdS is one of the short bandgap semiconductor materials with visible light absorption and suitable band structure in proton reduction.[29] Considering the low photocatalytic efficiency and instability of CdS itself,[30] co-catalysts like Pt,[31] NiS[32] particles were applied to enhance electron-hole separation and SO_3^{2-}/S^{2-} pair[33] for efficient hole scavenging. Bao[34] achieved a prominent high H_2 production efficiency of 60% using Pt-loaded nanoporous CdS nanostructures, in the presence of sacrificial reagents of Na_2SO_3 and Na_2S. The Pt nanocrystal photo-deposition condition on the CdS surface was further examined to have an inevitable impact on the Pt-CdS heterostructures. Rong Xu[35] showed that Pt-CdS photocatalyst had a much better H_2 generation activity with Pt in situ loaded in alkaline solution ($1300 \mu mol \cdot h^{-1}$), than that

deposited under acidic or neutral conditions (<50 $\mu mol \cdot h^{-1}$). This remarkedly high photocatalytic activity was attributed to the efficient Pt^{4+} species reduction (from precursor H_2PtCl_6) to metallic Pt^0 in alkaline condition, whereas in acidic or neutral solutions the deposition was not well finished. The pH related experiments were reexamined later with a more controlled Ni[36] or Pt[37] loading amount and solution pH. Ni nanoparticles decorated CdS nanorods[36] exhibited an external quantum efficiency of 53% under pH 14.7, with the presence of ethanol, overperforming those under lower pH. Hydroxyl ions and hydroxyl radicals were believed to function as a redox shuttle capable of relaying holes from CdS to ethanol. As was proposed by Feldmann, the redox potential of $OH^{\cdot}/OH^{-}$ catch up with CdS valence band edge at the pH around 14, which was well supported by the photocatalytic activity jump from pH 13 to pH 14. Similar jump was also observed for Pt decorated CdS nanorods[37], though at slightly lower pH (from 12 to 13). More recently, Amirav[38] achieved even higher H_2 generation efficiency up to 100%, employing CdSe-seeded CdS nanorod with Pt tips in an extreme pH of 15, water/isopropanol mixed solution. The reported high efficiency was attributed to the utilization of hydroxyl anion as a redox shuttle and it was confirmed by increased H_2 generation rate and suppressed trap recombination PL emission upon increasing pH of the reaction solution. Time-resolved PL and transient absorption spectra, however, was yet lacking in elucidating the charge-carrier behavior in similar steady state H_2 generation situations. In light of this, my work focused on examining the role of hydroxyl anion in the process of fast hole removing in CdS-Pt NRs, contributing to the better understanding of the oxidation side of solar water splitting.

3.2 Results and Discussion

Absorption and Emission Properties of CdS NRs and CdS-Pt NRs: TEM images of nanorods and Pt tipped nanorods displayed below show an average rod length 90 nm, diameter 5 nm for CdS-Pt NRs and 40 nm, 5 nm for CdSe/CdS-Pt NRs, respectively. CdSe/CdS and CdSe/CdS-Pt NRs are also included for comparison. Some bulb regions at the end of nanorods can be spotted that originate from the seeded-growth procedure has been reported previously.[39] The middle panel of Figure 3.1 presents static absorption and emission spectra of the nanorods and corresponding band alignments were also included for clarification. Typical CdSe/CdS NRs absorption has two prominent peaks at 410 nm and 460 nm, with a shoulder absorption at 480 nm. A much smaller CdSe seed absorption at 560 nm can be identified from the inserted graph. The unseeded CdS NRs have almost the same extinction features as the seeded ones, but for the seed absorption. Figure (e, f) illustrates the origination of the featured absorption peaks and corresponding photoluminescence spectra. Generally, there exists three distinct exciton states in the CdSe/CdS NRs with 400 nm excitation. The CdSe absorption of 560 nm corresponds to B3, with a red-shift from original CdSe seeds (511nm). This can be explained by the delocalization of electrons over CdSe and CdS, typical for a quasi-type II band alignment, which leads to a weaker overlap between the electrons and localized valence band holes of CdSe. Charge recombination of these electron-hole pairs gives rise to the most significant emission peak of CdSe/CdS NRs. Whereas a less obvious PL emission at 475 nm (after 100 fold magnification) and the more prominent 410 nm and 460 nm absorption peaks come from the B1 transition of the CdS rod region.[40] In addition to these pronounced features, there exists a shoulder emission at 480 nm of the PL emission for both CdSe/CdS

NRs and CdS NRs, which can be attributed to the lowest energy transition of the CdS bulb regions. Because of the fact that the CdS bulb is slightly bigger than the rod part in diameter, the CdS bulb has a smaller bandgap than CdS rod that accounts for a lower transition energy. Also depicted in the upper panel of Figure (e, f) is the hole trapping states on CdS rod surface and they result in a broad trapped electron-holes recombination emission from 500 to 900 nm for both CdSe/CdS NRs and CdS NRs.

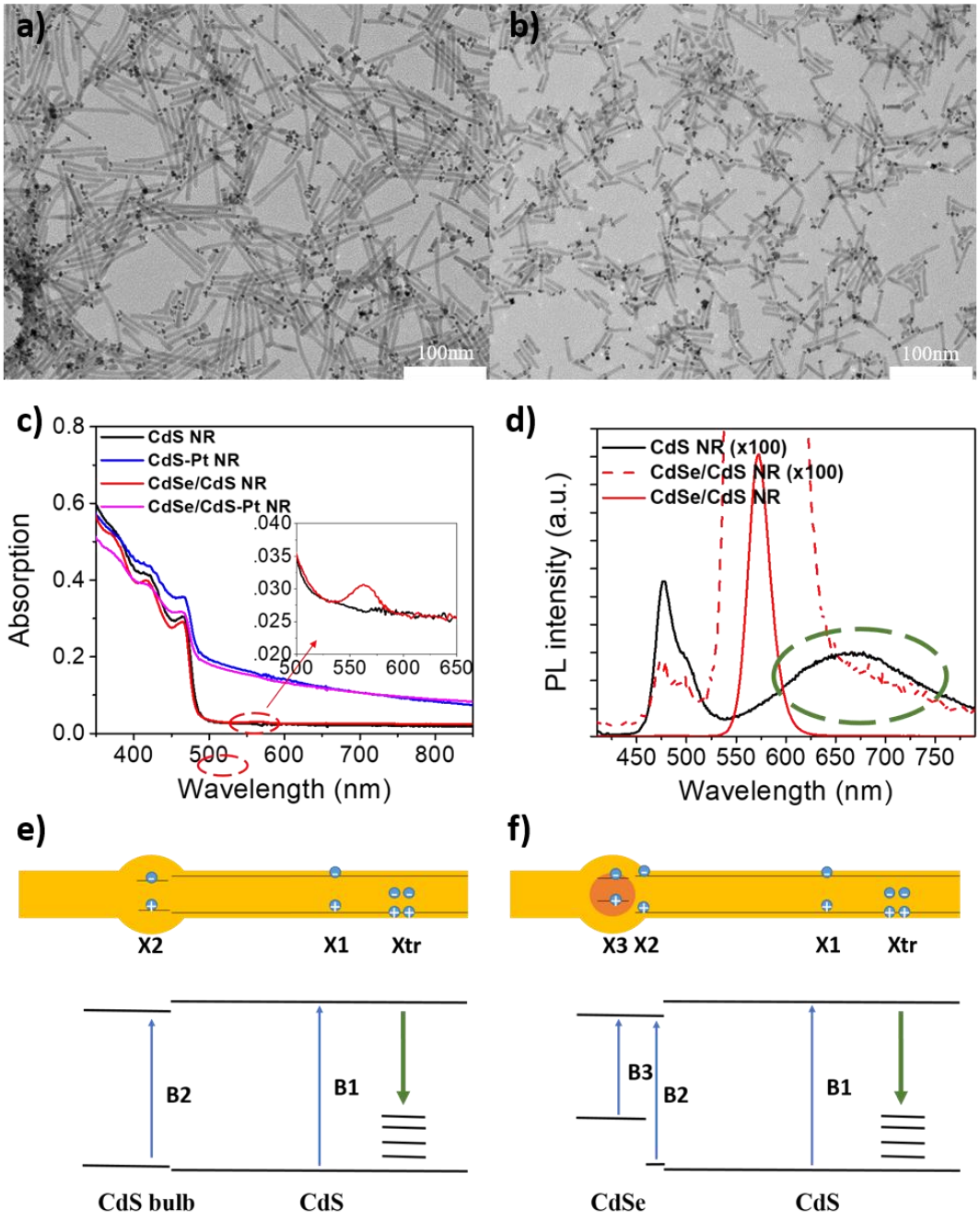

Figure 3.1 a, b) Transmission electronic microscopy (TEM) images of CdS-Pt NRs and CdSe/CdS-Pt NRs, respectively. c) Absorption spectra of the as-synthesized nanorods and Pt tipped nanorods. Inserted is the enlarged graph at a wavelength range from 500 to 650 nm. d) Steady state PL intensities of CdS NRs and CdSe/CdS NRs. e,f) Schematic illustration of existed distinct exciton

states (X1, X2, X3) in CdS NRs and CdSe/CdS NRs. Also shown below is the simplified schematic energy levels and possible band edge transitions.

The CdS-Pt NRs and CdSe/CdS-Pt NRs studied in this work were synthesized via the thermal reduction of Pt(II) acetylacetonate and heterogeneous Pt nucleation on the rod tips.[41] All Pt tipped NRs absorption can be well modeled as a linear combination of NRs and Pt nanoparticles contributions. As discussed above, the presence of different exciton states on CdSe/CdS and CdS NRs will make different electron dissociation path ways to Pt tips possible. Although these forward electron transfer steps are favorable for H_2 generation, the charge recombination, however, presents as a backward process. The pronounced recombination of delocalized electrons and localized holes in the CdSe/CdS NRs will actually place a disadvantage towards electron accumulation on Pt tips, which will be illustrated below.

Effect of pH and secondary electron donors on H_2 generation efficiency: H_2 generation efficiency comparison was first carried out under different pH (14 and 14.7). Before the H_2 generation reaction, the as-synthesized CdS-Pt NRs were transferred to aqueous solutions by replacing the phosphonate ligands with 3-Mercaptopropionic acid (MPA). The steady state H_2 production measurement was then carried out in a CdS-Pt NRs in water/ethanol mixed solution with volume ratio 4:1. The pH was adjusted with KOH pallets to either 14 or 14.7 for pH dependence control experiment. For secondary electron donor comparison experiment, isopropyl alcohol was chosen as an alternative to ethanol. Finally, difference in H_2 generation performance for CdS-Pt and CdSe/CdS-Pt NRs were compared. All the

samples were illuminated by 455 nm LED light (20 mW) and the H_2 amount was determined by gas chromatograph.

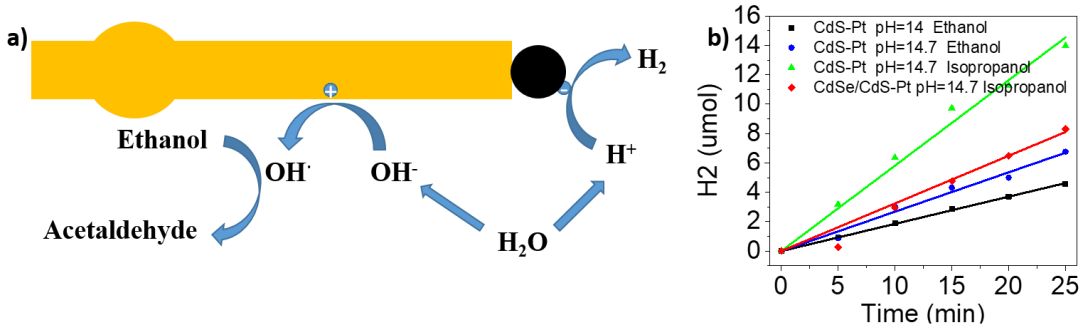

Figure 3.2 a) Schematic depicture of the photocatalytic H2 generation process b) H2 generation efficiency under different pH and second electron donors.

Before start, it is important to introduce the working principle in this H_2 generation system. As shown in Figure 3.2(a), upon 455 nm laser illumination, photoexcited holes oxidize hydroxyl anion and the hydroxyl radical pass on the positive charge to ethanol which turns to acetaldehyde. On the Pt side, hydrogen irons capture electrons from the Pt tip to form H_2 molecules.

Table 3.1 H2 generation efficiencies under different conditions

	CdS-Pt	**CdS-Pt**	**CdS-Pt**	**CdSe/CdS-Pt**
pH	14	14.7	14.7	14.7
Secondary electron donor	Ethanol	Ethanol	Isopropanol	Isopropanol
Rate (umol/h)	11.9	19.5	34.9	19.5
EQE (%)	9.5	18.5	29.3	16.3
IQE (%)	24.5	45.9	72.5	42.3

Table 3.1 shows that H_2 generation efficiencies of the described reaction protocol yield the highest (external quantum efficiency (EQE) equals to 29.3%) when CdS-Pt NRs were used as the functional photocatalytic material with isopropanol as the secondary electron donor

in a pH = 14.7 solution. The internal quantum efficiency (IQE) of the system is even higher after subtracting the absorption part of Pt nanoparticles. Solution pH makes a big difference such that the CdS-Pt/Ethanol complex with pH 14.7 (5M KOH) produced more H_2 than that with pH 14 (1M KOH) at a given time. The increased H_2 generation was attributed to faster hole removal rate when the hydroxyl anion concentration was increased. The high pH was then applied to the comparison of different

secondary electron donors and CdSe seeded or unseeded nanorods. It was clear that the reaction was enhanced when ethanol was replaced by isopropanol, since by forming the product acetone, isopropanol tends to be oxidized more easily than ethanol. As for the difference in seeded or unseeded CdS NRs, previous comparisons have reported higher quantum efficiency for CdSe/CdS-Pt NRs heterostructures,[42] than CdS-Pt NRs. The higher efficiency is often attributed to the quasi-type II band alignment of this dot-in-rod structure that can promote charge separation between the CdSe seed and CdS rod. In order to testify the effects of CdSe seeds, CdS-Pt NRs and CdSe/CdS-Pt NRs were compared, with isopropanol and a solution pH of 14.7. As can be seen in Figure 3.2(b) and also Table 3.1, CdS-Pt NRs actually yielded a much higher efficiency than CdSe/CdS-Pt NRs. This result combined with previous work by our group[43] indicates that electron-hole separation is not the efficiency-limiting factor in this heterostructured materials. Further research including a detailed pH-dependence experiment over a large pH range (8.0 – 14.7) of these two kind of nanorods will be conducted to examine the role of CdSe seeds.

Time resolved PL lifetime and TA study: Charge separation and recombination kinetics of the CdS-Pt and CdSe/CdS-Pt NRs were studied by time resolved fluorescence decay and

transient absorption measurements. Figure 3.3 shows the preliminary data at present. From the panel (a) we can see there is an obvious upshift upon high pH range in CdS NRs aqueous solutions. This upshift was caused by the aggregates scattering of the CdS NRs that in turn came from the instability of these nanorods in very alkaline condition. The presence of large amount of hydroxyl anions would affect the surface passivation of

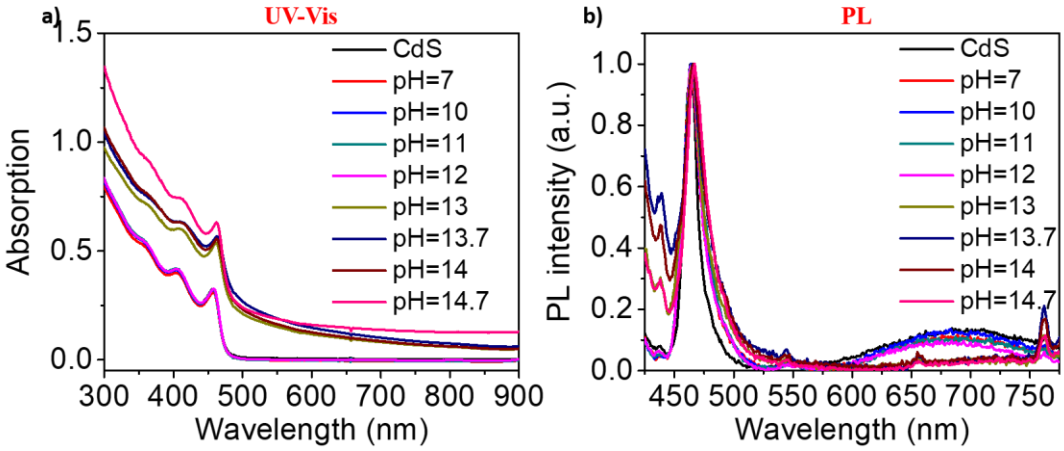

Figure 3.3 a) UV-Vis absorption of the CdS NRs after ligand exchange to aqueous solution. b) Steady state PL intensity of CdS NRs under different pH.

nanorods, finally leading to aggregation. Interestingly, however, the aggregation of nanorods didn't seem to lower the photocatalytic performance, which has been noticed in a previous literature reporting the shortening and aggregating of CdS-Pt NRs under photocatalytic situations while maintaining H_2 generation activity.[44] Figure 3.3(b) shows the static photoluminescence of CdS NRs in different pH solutions. The band edge emission at about 470 nm were normalized in order for better comparison of the trap states recombination emission. The trap emission decreased gradually upon increased pH and experienced a sudden jump at pH 13, which was also the point when CdS NRs started to aggregate. Consistent with the H_2 generation experiment, with the increasing of pH, photo-

excited holes would be fast removed and so reduce the possibility of CB electron – trapped hole recombination. The PL intensity of the trap emission of CdS NRs will correspondingly decrease, whereas the intrinsic emission of CdS would experience moderate change.

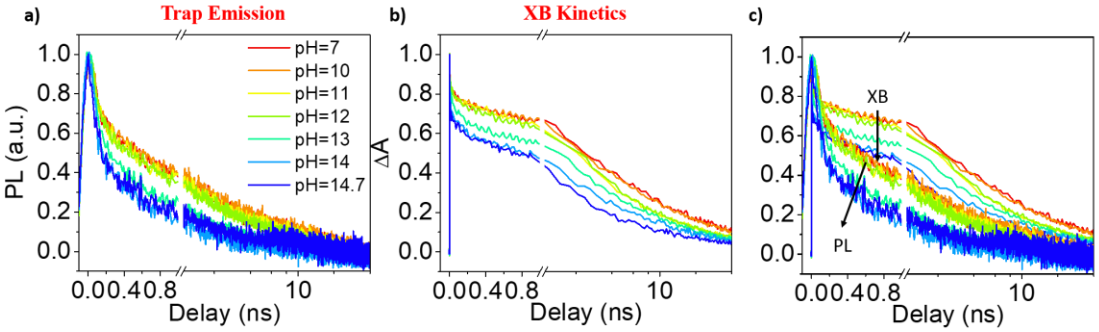

Figure 3.4 a) PL lifetime of CdS trap emission. b) Exciton bleach (XB) feature of CdS NRs probed at 466 nm, in different pH solutions. c) Merged graph of a) & b) for better comparison.

TA and PL lifetime kinetics in Figure 3.4 provide further evidence of this fast hole removal. In the combined feature as shown in Figure 3.4(c), we can observe fast decay of both electron and PL lifetime, at a very early stage upon excitation. The fact that PL decay curve was limited by the instrumental response made it hard to compare the behavior of photo excited electrons and holes. After a few hundred picoseconds, however, it is clear that PL decays much faster than electrons. Since PL trace involves both the electron decay and hole removal, we can deduce that even though electron decay account for part of the PL decay, the overall PL decay was caused by the fast hole removing. More importantly, with the increase of solution pH, trap emission had an accelerated decay kinetics which corresponds to a more efficient hole removing process.

3.3 Conclusion

Semiconductor nanomaterials based H_2 generation has been regarded as a promising approach to solving the world energy crisis for their suitable band edge energetics and tunable optical properties. Pt-tipped CdS nanorods serve as a model material integrating metallic tips, such as Pt, as a cocatalyst and CdS nanorod as light absorbing domain. The efficiency of H_2 generation under these semiconductor-metal heterostructures are often limited by the slow hole removing rate and the ensuing high charge recombination rates. By utilizing hydroxyl anion as an electron donor, we showed efficient hole removing rate upon illumination (455nm) of the CdS-Pt NRs and achieved an external quantum efficiency (EQE) of 29.3% and H_2 generation rate of 34.9 umol/h. CdSe/CdS-Pt NRs were also examined under the same situation to further demonstrate the effect of fast hole removal, rather than confining inside CdSe seed.

3.4 Sample Preparation

Synthesis of CdSe seeds: Wurtzite CdSe seeds used for the nanorod growth were synthesized following a literature procedure.[45] Typically, 0.06 g Cadmium Oxide (CdO), 0.28 g Octadecylphosphonic acid (ODPA) and 3 g Trioctylphosphine oxide (TOPO) were mixed in a 50 ml three-neck flask and degassed under vacuum for half an hour at 150 ℃. After degassing, the system was changed to argon flow and the temperature was allowed to raise to 350 ℃ to fully dissolve CdO. 1.8 ml Trioctylphosphine (TOP) was injected and selenium (Se) precursor (0.058g Se + 0.36g TOP) was swiftly injected after the temperature recovered to 350℃. The reaction was immediately stopped by removing the heating mantle,

when the desired nanoparticle size formed. The CdSe seed was precipitated by ethanol/toluene for several times and redissolved in chloroform for further use.

Synthesis of CdS seeds: OA-capped wurtzite CdS seeds were synthesized according to a previous method.[46] Typically, 0.077 g Cadmium Oxide (CdO), 0.5 ml Oleic Acid (OA), 14.5 ml Octadecene (ODE) were mixed in a 50 ml three-neck flask and degassed at 105 ℃ for half an hour. After degassing, the system was changed to argon flow and the temperature was allowed to raise to 280 ℃ to fully dissolve CdO. Then the temperature was lowered to 250 ℃ and sulfur (S) precursor (0.010g S + 0.6mlODE) was swiftly injected. After 70s, the reaction was stopped by removing the heating mantle and quenched in a water bath. The CdS seed was washed with ethanol/toluene for several times and redissolved in chloroform.

Synthesis of CdSe/CdS NRs and CdS NRs: NRs used in this study was synthesized by a seeded-growth procedure.[45] CdSe (with its first excitonic peak at 511 nm) and CdS quantum dots (with its first excitonic peak at 362 m) were used as the seed for rod growth. The concentration of these quantum dots were calculated according published extinction coefficient.[15] For a NR growth, 0.06 g Cadmium Oxide (CdO), 0.29 g Octadecylphosphonic acid (ODPA), 0.08 g hexylphosphonic acid (HPA) and 3 g Trioctylphosphine oxide (TOPO) were mixed in a 50 ml three-neck flask and degassed under vacuum for half an hour at 150 ℃. After degassing, the system was changed to argon flow and the temperature was allowed to raise to 350 ℃ to fully dissolve CdO, followed by 1.8 ml Trioctylphosphine (TOP) injection. In a separated container, sulfur injection solution (0.12g S in 1.8ml TOP) was mixed with 8×10^{-8} mol CdSe or CdS QDs. When the temperature recovered to 350℃, the seed-containing sulfur precursor solution was swiftly

injected. The reaction was allowed to react for 5 min before stopped by removing the heating mantle. The NRs was precipitated by ethanol/toluene for several times and redissolved in chloroform for further use.

Synthesis of platinum (Pt) tipped CdSe/CdS NRs and CdS NRs: One end growth of Pt tip on NRs were synthesized according to a reported procedure.[47] Typically, 0.2 ml Oleic Acid (OA), 0.2 ml Oleylamine (OLA), 0.043 g 1,2-hexadecanediol (HDDO) and 10 ml Diphenyl Ether was mixed in a 50 ml three-neck flask and degassed under vacuum for half an hour at 80 ℃.After degassing, the system was changed to argon flow and the temperature was allowed to raise to 200 ℃. 15 mg Pt(II) acetylacetonate was mixed with a suspension of NRs in Dichlorobenzene and sonicated for a few minutes to dissolve the Pt precursor. After the flask temperature stabilized at 200 ℃, the NRs-containing Pt precursor solution was swiftly injected. The reaction was allowed to proceed for 7 min before quenched by water bath. The products was precipitated by ethanol/toluene for several times and redissolved in chloroform.

Ligand exchange for CdSe/CdS NRs and CdS NRs: The original ligands on NRs were replaced by 3-Mercaptopropionic acid (MPA). Typically, 30 ul MPA and 10 ml of 0.4 M KOH aqueous solution were added to 2 ml chloroform solutions of NRs. The mixture was vigorously stirred for about 1 h and then left to separate into two layers. The upper layer was taken out and added with 10 ml methanol to precipitate out the NRs. The precipitates were finally redissolved in water.

4. Acknowledgements

I want to first acknowledge my Advisor Dr. Tianquan (Tim) Lian for his three years' support and guidance. I really appreciate Dr. Lian would meet with me every week to discuss my research progress and provide me valuable suggestions on future work. I also want to acknowledge my committee members Dr. Brian Dyer and Dr. Michael C. Heaven for their help and advice in all these years, through my second year report to my graduation today.

I want to thank Jia Song and Zihao Xu for their help in the data processing and all other group members for all the cooperation and friendship with me.

5. References

1. Pasten, C.; Santamarina, J. C., Energy and quality of life. *Energy Policy* **2012,** *49,* 468-476.

2. Fontecave, M., Energy for a Sustainable World. From the Oil Age to a Sun-Powered Future. Von Nicola Armaroli und Vincenzo Balzani. *Angewandte Chemie* **2011,** *123* (30), 6836-6837.

3. Chen, X.; Shen, S.; Guo, L.; Mao, S. S., Semiconductor-based Photocatalytic Hydrogen Generation. *Chemical reviews* **2010,** *110* (11), 6503-6570.

4. Habisreutinger, S. N.; Schmidt-Mende, L.; Stolarczyk, J. K., Photocatalytic Reduction of CO2 on TiO2 and Other Semiconductors. *Angewandte Chemie International Edition* **2013,** *52* (29), 7372-7408.

5. Brus, L., Electronic wave functions in semiconductor clusters: experiment and theory. *The Journal of Physical Chemistry* **1986,** *90* (12), 2555-2560.

6. Brus, L. E., Electron–electron and electron-hole interactions in small semiconductor crystallites: The size dependence of the lowest excited electronic state. *The Journal of Chemical Physics* **1984,** *80* (9), 4403-4409.

7. White, J. L.; Baruch, M. F.; Pander Iii, J. E.; Hu, Y.; Fortmeyer, I. C.; Park, J. E.; Zhang, T.; Liao, K.; Gu, J.; Yan, Y.; Shaw, T. W.; Abelev, E.; Bocarsly, A. B., Light-Driven Heterogeneous Reduction of Carbon Dioxide: Photocatalysts and Photoelectrodes. *Chemical reviews* **2015,** *115* (23), 12888-12935.

8. Kumar, B.; Llorente, M.; Froehlich, J.; Dang, T.; Sathrum, A.; Kubiak, C. P., Photochemical and Photoelectrochemical Reduction of CO2. *Annual Review of Physical Chemistry* **2012,** *63* (1), 541-569.

9. Barton, E. E.; Rampulla, D. M.; Bocarsly, A. B., Selective Solar-Driven Reduction of CO2 to Methanol Using a Catalyzed p-GaP Based Photoelectrochemical Cell. *Journal of the American Chemical Society* **2008,** *130* (20), 6342-6344.

10. Yan, Y.; Zeitler, E. L.; Gu, J.; Hu, Y.; Bocarsly, A. B., Electrochemistry of Aqueous Pyridinium: Exploration of a Key Aspect of Electrocatalytic Reduction of CO2 to Methanol. *Journal of the American Chemical Society* **2013,** *135* (38), 14020-14023.

11. Fang, Y.; Flake, J. C., Electrochemical Reduction of CO2 at Functionalized Au Electrodes. *Journal of the American Chemical Society* **2017,** *139* (9), 3399-3405.

12. Keith, J. A.; Carter, E. A., Theoretical Insights into Pyridinium-Based Photoelectrocatalytic Reduction of CO2. *Journal of the American Chemical Society* **2012,** *134* (18), 7580-7583.

13. Lim, C.-H.; Holder, A. M.; Musgrave, C. B., Mechanism of Homogeneous Reduction of CO2 by Pyridine: Proton Relay in Aqueous Solvent and Aromatic Stabilization. *Journal of the American Chemical Society* **2013,** *135* (1), 142-154.

14. Chen, J.; Wu, K.; Rudshteyn, B.; Jia, Y.; Ding, W.; Xie, Z. X.; Batista, V. S.; Lian, T., Ultrafast Photoinduced Interfacial Proton Coupled Electron Transfer from CdSe Quantum Dots to 4,4'-Bipyridine. *Journal of the American Chemical Society* **2016,** *138* (3), 884-92.

15. Yu, W. W.; Qu, L.; Guo, W.; Peng, X., Experimental Determination of the Extinction Coefficient of CdTe, CdSe, and CdS Nanocrystals. *Chemistry of Materials* **2003,** *15* (14), 2854-2860.

16. Pannwitz, A.; Wenger, O. S., Proton coupled electron transfer from the excited state of a ruthenium(ii) pyridylimidazole complex. *Physical Chemistry Chemical Physics* **2016,** *18* (16), 11374-11382.

17. Harriman, A.; Millward, G. R.; Neta, P.; Richoux, M. C.; Thomas, J. M., Interfacial electron-transfer reactions between platinum colloids and reducing radicals in aqueous solution. *The Journal of Physical Chemistry* **1988,** *92* (5), 1286-1290.

18. Song, N.; Zhu, H.; Jin, S.; Zhan, W.; Lian, T., Poisson-Distributed Electron-Transfer Dynamics from Single Quantum Dots to C60 Molecules. *ACS Nano* **2011,** *5* (1), 613-621.

19. Huang, J.; Huang, Z.; Jin, S.; Lian, T., Exciton Dissociation in CdSe Quantum Dots by Hole Transfer to Phenothiazine. *The Journal of Physical Chemistry C* **2008,** *112* (49), 19734-19738.

20. Morris-Cohen, A. J.; Frederick, M. T.; Cass, L. C.; Weiss, E. A., Simultaneous Determination of the Adsorption Constant and the Photoinduced Electron Transfer Rate for a Cds Quantum Dot–Viologen Complex. *Journal of the American Chemical Society* **2011,** *133* (26), 10146-10154.

21. Fang, Z.; Wang, Y.; Song, J.; Sun, Y.; Zhou, J.; Xu, R.; Duan, H., Immobilizing CdS quantum dots and dendritic Pt nanocrystals on thiolated graphene nanosheets toward highly efficient photocatalytic H2 evolution. *Nanoscale* **2013,** *5* (20), 9830-9838.

22. Wu, K.; Liang, G.; Shang, Q.; Ren, Y.; Kong, D.; Lian, T., Ultrafast Interfacial Electron and Hole Transfer from CsPbBr3 Perovskite Quantum Dots. *Journal of the American Chemical Society* **2015,** *137* (40), 12792-12795.

23. Zuttel, A.; Remhof, A.; Borgschulte, A.; Friedrichs, O., Hydrogen: the future energy carrier. *Philosophical transactions. Series A, Mathematical, physical, and engineering sciences* **2010,** *368* (1923), 3329-42.

24. Arrhenius, S., XXXI. On the influence of carbonic acid in the air upon the temperature of the ground. *Philosophical Magazine Series 5* **1896,** *41* (251), 237-276.

25. Hubbert, M. K., Nuclear Energy and the Fossil Fuel. American Petroleum Institute: 1956.

26. Fujishima, A.; Honda, K., Electrochemical Photolysis of Water at a Semiconductor Electrode. *Nature* **1972,** *238* (5358), 37-38.

27. Ni, M.; Leung, M. K. H.; Leung, D. Y. C.; Sumathy, K., A review and recent developments in photocatalytic water-splitting using for hydrogen production. *Renewable and Sustainable Energy Reviews* **2007,** *11* (3), 401-425.

28. Kato, H.; Asakura, K.; Kudo, A., Highly Efficient Water Splitting into H2 and O2 over Lanthanum-Doped NaTaO3 Photocatalysts with High Crystallinity and Surface Nanostructure. *Journal of the American Chemical Society* **2003,** *125* (10), 3082-3089.

29. Serpone, N.; Borgarello, E.; Gratzel, M., Visible light induced generation of hydrogen from H2S in mixed semiconductor dispersions; improved efficiency through inter-particle electron transfer. *Journal of the Chemical Society, Chemical Communications* **1984,** (6), 342-344.

30. Kudo, A.; Miseki, Y., Heterogeneous photocatalyst materials for water splitting. *Chemical Society reviews* **2009,** *38* (1), 253-278.

31. Dukovic, G.; Merkle, M. G.; Nelson, J. H.; Hughes, S. M.; Alivisatos, A. P., Photodeposition of Pt on Colloidal CdS and CdSe/CdS Semiconductor Nanostructures. *Advanced materials* **2008,** *20* (22), 4306-4311.

32. Zhang, W.; Wang, Y.; Wang, Z.; Zhong, Z.; Xu, R., Highly efficient and noble metal-free NiS/CdS photocatalysts for H2 evolution from lactic acid sacrificial solution under visible light. *Chemical Communications* **2010,** *46* (40), 7631-7633.

33. Buehler, N.; Meier, K.; Reber, J. F., Photochemical hydrogen production with cadmium sulfide suspensions. *The Journal of Physical Chemistry* **1984,** *88* (15), 3261-3268.

34. Bao, N.; Shen, L.; Takata, T.; Domen, K., Self-Templated Synthesis of Nanoporous CdS Nanostructures for Highly Efficient Photocatalytic Hydrogen Production under Visible Light. *Chemistry of Materials* **2008,** *20* (1), 110-117.

35. Wang, Y.; Wang, Y.; Xu, R., Photochemical Deposition of Pt on CdS for H2 Evolution from Water: Markedly Enhanced Activity by Controlling Pt Reduction Environment. *The Journal of Physical Chemistry C* **2013,** *117* (2), 783-790.

36. Simon, T.; Bouchonville, N.; Berr, M. J.; Vaneski, A.; Adrović, A.; Volbers, D.; Wyrwich, R.; Döblinger, M.; Susha, A. S.; Rogach, A. L.; Jäckel, F.; Stolarczyk, J. K.; Feldmann, J., Redox shuttle mechanism enhances photocatalytic H2 generation on Ni-decorated CdS nanorods. *Nature materials* **2014,** *13* (11), 1013-1018.

37. Schneider, J.; Vaneski, A.; Pesch, G. R.; Susha, A. S.; Yang Teoh, W.; Rogach, A. L., Enhanced hydrogen evolution rates at high pH with a colloidal cadmium sulphide–platinum hybrid system. *APL Materials* **2014,** *2* (12), 126102.

38. Kalisman, P.; Nakibli, Y.; Amirav, L., Perfect Photon-to-Hydrogen Conversion Efficiency. *Nano letters* **2016**.

39. Wu, K.; Rodríguez-Córdoba, W. E.; Liu, Z.; Zhu, H.; Lian, T., Beyond Band Alignment: Hole Localization Driven Formation of Three Spatially Separated Long-Lived Exciton States in CdSe/CdS Nanorods. *ACS Nano* **2013,** *7* (8), 7173-7185.

40. Wu, K.; Zhu, H.; Liu, Z.; Rodríguez-Córdoba, W.; Lian, T., Ultrafast Charge Separation and Long-Lived Charge Separated State in Photocatalytic CdS–Pt Nanorod Heterostructures. *Journal of the American Chemical Society* **2012,** *134* (25), 10337-10340.

41. Mokari, T.; Rothenberg, E.; Popov, I.; Costi, R.; Banin, U., Selective Growth of Metal Tips onto Semiconductor Quantum Rods and Tetrapods. *Science* **2004,** *304* (5678), 1787-1790.

42. Amirav, L.; Alivisatos, A. P., Photocatalytic Hydrogen Production with Tunable Nanorod Heterostructures. *The Journal of Physical Chemistry Letters* **2010,** *1* (7), 1051-1054.

43. Wu, K.; Chen, Z.; Lv, H.; Zhu, H.; Hill, C. L.; Lian, T., Hole Removal Rate Limits Photodriven H2 Generation Efficiency in CdS-Pt and CdSe/CdS-Pt Semiconductor Nanorod–Metal Tip Heterostructures. *Journal of the American Chemical Society* **2014,** *136* (21), 7708-7716.

44. Berr, M. J.; Wagner, P.; Fischbach, S.; Vaneski, A.; Schneider, J.; Susha, A. S.; Rogach, A. L.; Jäckel, F.; Feldmann, J., Hole scavenger redox potentials determine quantum efficiency and stability of Pt-decorated CdS nanorods for photocatalytic hydrogen generation. *Applied Physics Letters* **2012,** *100* (22), 223903.

45. Carbone, L.; Nobile, C.; De Giorgi, M.; Sala, F. D.; Morello, G.; Pompa, P.; Hytch, M.; Snoeck, E.; Fiore, A.; Franchini, I. R.; Nadasan, M.; Silvestre, A. F.; Chiodo, L.; Kudera, S.; Cingolani, R.; Krahne, R.; Manna, L., Synthesis and Micrometer-Scale Assembly of Colloidal CdSe/CdS Nanorods Prepared by a Seeded Growth Approach. *Nano letters* **2007,** *7* (10), 2942-2950.

46. Yu, W. W.; Peng, X., Formation of High-Quality CdS and Other II–VI Semiconductor Nanocrystals in Noncoordinating Solvents: Tunable Reactivity of Monomers. *Angewandte Chemie International Edition* **2002,** *41* (13), 2368-2371.

47. Habas, S. E.; Yang, P.; Mokari, T., Selective Growth of Metal and Binary Metal Tips on CdS Nanorods. *Journal of the American Chemical Society* **2008,** *130* (11), 3294-3295.